International Journal of Thermal Sciences 49 (2010) 1031–1041

Contents lists available at ScienceDirect

International Journal of Thermal Sciences

journal homepage: www.elsevier.com/locate/ijts

Thermal analysis of a 2-D heat recovery system using porous media including lattice Boltzmann simulation of fluid flow

E. Jahanshahi Javaran, S.A. Gandjalikhan Nassab*, S. Jafari

Mechanical Engineering Department, School of Engineering, Shahid Bahonar University, Kerman, Iran

ARTICLE INFO

Article history:
Received 13 May 2009
Received in revised form
6 December 2009
Accepted 9 December 2009
Available online 20 January 2010

Keywords:
Lattice Boltzmann method
Porous medium
Discrete ordinates method
Heat recovery

ABSTRACT

The present work deals with the fluid flow simulation and thermal analysis of a two-dimensional heat recovery system using porous media. A basic high-temperature flow system is considered in which a high-temperature non-radiating gas flows through a random porous matrix. The porous medium, in addition to its convective heat exchange with the gas, may absorb, emit and scatter thermal radiation. It is desirable to have large amount of radiative heat flux from the porous segment in the upstream direction (towards the thermal system). The lattice Boltzmann method (LBM) is used to simulate fluid flow in the porous medium. The gas and solid phases are considered in non-local thermal equilibrium, and separate energy equations are applied to these phases. Convection, conduction and radiation heat transfers take place simultaneously in solid phase, but in the gas flow, heat transfer occurs by conduction and convection. In order to analyze the thermal characteristics of the heat recovery system, volume-averaged velocities through the porous matrix obtained by LBM are used in the gas energy equation and then the coupled energy equations for gas and porous medium are numerically solved using finite difference method. For computing of radiative heat flux in the porous medium, discrete ordinates method is used to solve the radiative transfer equation. Finally the effect of various parameters on the performance of porous heat recovery system is studied.

1. Introduction

Heat transfer efficiency enhancement in high temperature systems is a great desire for engineers. Over the years, many researchers have studied energy recovery by means of porous media to capture waste heat from exhaust gases [1,2]. The mechanism of this phenomenon is based on energy conversion between gas enthalpy and thermal radiation. This heat exchange consists of two-heat transfer processes: (a) convection between gas flow and porous media due to the large surface area of the porous medium and high heat transfer coefficient, (b) radiation from the porous medium whose emissive power is much higher than that of gases. A schematically illustration of this process is shown in Fig. 1. The similar phenomenon is used in porous radiant burners and leaded to increase in their efficiencies [3]. There are several studies about heat recovery in thermal systems by means of porous media. A study by Echigo [1] shows that, with an appropriate choice of the optical thickness of the permeable medium, up to 60 percent of non-radiating gas energy can be saved owing to the converted radiation. In that study, the gas scattering effect was neglected. Thermal insulation in steady high-temperature flow systems was studied by Wang and Tien [4] using a two-flux radiation model and the scattering effect of the porous layer was also considered in computations. Yoshida et al. [5] investigated the transient characteristics of heat transfer in porous media. In that work, because of high porosity of the porous media, the conduction heat transfer in the radiative converter was neglected. In the non-radiating gas flow analysis, it was assumed that conduction and convection occur simultaneously and integral method was used to obtain the net radiative heat flux in the porous matrix. Transient heat transfer characteristics of an energy recovery system using porous media was investigated by Gandjalikhan Nassab [6] in which the two-flux radiation model was used to calculate the radiative fluxes. Based on energy conversion phenomena between gas enthalpy and thermal radiation, new types of gas-to-gas heat exchanger have been proposed and analyzed by many investigators [7,8]. In a recent study, a multi-layered type of gas-to-gas heat exchanger was analyzed by the second author. This system has five porous layers consisting of two high temperature (HT) and three heat recovery (HR) sections. In HT sections, the enthalpy of the flowing high temperature gas flow is converted to thermal radiation and reverse phenomenon takes place in HR sections by converting thermal

* Corresponding author.
E-mail address: ganjali2000@yahoo.com (S.A. Gandjalikhan Nassab).

1290-0729/$ – see front matter © 2009 Elsevier Masson SAS. All rights reserved.
doi:10.1016/j.ijthermalsci.2009.12.004

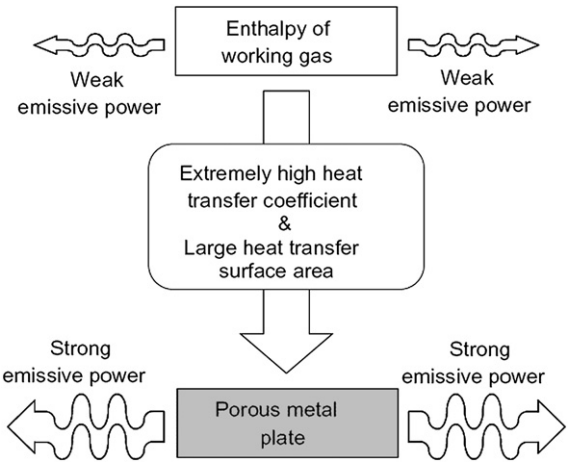

Fig. 1. Effective energy conversion mechanism [1].

radiation into gas enthalpy. By this method, the low temperature air flow into the heat exchanger is heated along three steps. In that work, the one-dimensional conduction, convection and radiation heat transfer were taken place simultaneously in both gas and solid phases [7], and the two-flux radiation model was used for the computation of radiative fluxes through porous layers, such that the gas radiation effect was also considered into account. It was shown that porous heat exchanger with high optical thickness has a very high efficiency. In all of the above works, for obtaining the gas and porous temperature distributions along the porous layer, the gas and porous energy equations was solved numerically, such that the convective term in gas energy equation was considered by assuming a simple plug flow through porous matrix. Other important aspect in porous media is fluid flow simulation. Because of the complex geometry and random nature of porous media, simulation of fluid flow by means of Navier–Stokes equations is difficult. In recent years, the lattice Boltzmann method has developed into an alternative and promising numerical scheme for simulating fluid flows and modeling physics in fluids. The scheme is particularly successful in fluid flow applications involving interfacial dynamics and complex boundaries [9,10].

The first LBM simulation of the fluid flow in porous media was carried out by Foti and Succi [11]. In that work, Darcy's law was recovered and a preliminary estimation of the permeability presented. Numerical simulations of the lattice Boltzmann equation in three-dimensional porous geometries constructed by the random positioning penetrable spheres of equal radii were investigated by Cancelliere et al. [12] and methods for calculating the permeability were presented. Koponen et al. [13] used the lattice Boltzmann method on a massively parallel computer to solve ab initio the permeability of a large random 3D fiber web as a function of its porosity in a large porosity range. They found that the exponential dependence on porosity of permeability in a wide range of porosities is a generic feature of fibrous porous materials, independent of whether they are random or not.

Guo and Zhao [14] have proposed the lattice Boltzmann model for incompressible flow in porous media. In that work, the influence of porous medium was incorporated into the model by introducing a newly defined equilibrium distribution function and adding a force term into the lattice Boltzmann equation and fluid-solid interactions is modeled by the force term. Pan et al. [15] quantitatively evaluated the capability and accuracy of the lattice Boltzmann equation (LBE) for modeling flow through porous media. In that work, several fluid-solid boundary conditions were investigated. They also conducted a comparative study of LBE models with the multiple-relaxation time (MRT) and Bhatnagar-Gross-Krook (BGK) single-relaxation time (SRT) collision operators and found that MRT-LBE model is superior to the BGK-LBE model. Fluid flow in 2-D random porous media was simulated at pore level using the LBM by Nabovati and Sousa [16]. They showed that for the same porosity, the permeability of the random porous media is lower than the permeability of the regularly ordered medium. The permeability, independently of the porous medium structure, varies exponentially with the porosity. Wei–Wei Yan et al. [17] have studied the porous flow through low head loss biofilter medium using LBM. They showed that LBM is capable of solving the problems that fluids flowing through porous media with constant pressure difference. Three-dimensional fluid flow simulations in fibrous media were conducted using the SRT LBM by Nabovati et al. [18]. The fibrous media were constructed by random placement of cylindrical fibers, with random orientations, within the computational domain. The radius, curvature and length of the fibers were varied systematically. It was found that fiber curvature has a negligible impact on the permeability of the medium. To the best of author's knowledge, the thermal characteristics of porous heat recovery system have not been obtained by solving the flow equation using LBM.

In the present study, to determine the performance of an energy recovery system by porous media, simulation of fluid flow in two-dimensional random porous medium at pore level scale is done using lattice Boltzmann method. In the thermal analysis of this system, the gas and solid phase are assumed in non-local thermal equilibrium, thus separate energy equations are used for the two phases. In the numerical simulation of the present heat recovery system, three modes of heat transfer take place in the solid phase whereas in the gas phase, heat transfer occurs by conduction and convection and the gas radiation effect is neglected. Thereby, the governing energy equations in thermal analysis of the heat recovery system are two energy equations for the gas and solid phases and radiative energy equation for solid phase. These equations are simultaneously solved to determine thermal behavior of the system. The discrete ordinates method is used to solve the radiative transfer equation. Two energy equations are iteratively solved using line by line TDMA. The accuracy of the theoretical model and the numerical code is confirmed by comparison with the theoretical results of other investigators and good agreement is found.

2. Simulation of fluid flow by means of lattice Boltzmann method

2.1. A general overview of the lattice Boltzmann method

In this work, the lattice Boltzmann equation with the multiple-relaxation time (MRT) is used [15,19],

$$\mathbf{f}(x_i + e\delta t, t + \delta t) = \mathbf{f}(x_i, t) - M^{-1} \cdot \widehat{S} \cdot [\mathbf{m} - \mathbf{m}^{eq}(\rho, u)](x_i, t) \quad (1)$$

In which ρ and u are the macroscopic density and velocity respectively, the bold face symbols such as $\boldsymbol{f}$ stand for 9-component vectors, 9 is the number of discrete velocities, as follows:

$$\mathbf{f} = (f_0, f_1, \ldots\ldots, f_8)^T \quad (2)$$

$$\mathbf{f}(x_i + e_\alpha \delta t) = (f_0(x_i), f_1(x_i + e_1\delta t), \ldots\ldots, f_8(x_i + e_8\delta t))^T \quad (3)$$

$$\mathbf{m} = (m_0, m_1, \ldots\ldots, m_8) \quad (4)$$

$$\mathbf{m}^{eq} = (m_0^{eq}, m_1^{eq}, \ldots\ldots, m_8^{eq}) \quad (5)$$

where T denotes the transpose operator. In Eq. (1) $\boldsymbol{f}$ is the 9-component vector of the discrete distribution functions, $\boldsymbol{m}$ and $\boldsymbol{m}^{eq}$ are 9-component vectors of moments and their equilibria, M is the transformation matrix and $\widehat{S}$ is the diagonal matrix of relaxation rates.

The nine-velocity square lattice Boltzmann (D_2Q_9) model has widely and successfully been used for simulating two-dimensional flows. In the (D_2Q_9) model, e_α denotes the discrete velocity set, namely,

$$e_0 = (0,0) \tag{6-a}$$

$$e_\alpha = (\pm 1, 0)c \text{ and } (0,\pm 1)c \quad \text{for } \alpha = 1,2,3,4 \tag{6-b}$$

$$e_\alpha = (\pm 1, \pm 1)c \quad \text{for } \alpha = 5,6,7,8 \tag{6-c}$$

Where $c = \delta x/\delta t$, δx and δ_t are the lattice spacing and the time increment which are assumed to be unity.

The moments are arranged in the following order:

$$\mathbf{m} = \left(\rho, e, \varepsilon, j_x, q_x, j_y, q_y, p_{xx}, p_{xy}\right)^T \tag{7}$$

Where $m_0 = \rho$ is the density, $m_1 = e$ is related to the total energy, $m_2 = \varepsilon$ is related to energy square, $(m_3,m_5) = (j_x,j_y) = \rho(u_x,u_y)$ is the flow momentum, $(m_4,m_6) = (q_x,q_y)$ is related to the heat flux, and $m_7 = p_{xx}$ and $m_8 = p_{xy}$ are related to the diagonal and off-diagonal components of the stress tensor, respectively.

The macroscopic density and momentum on each lattice node are calculated using the following equations:

$$\rho = \sum_{\alpha=0}^{8} f_\alpha \tag{8}$$

$$\mathbf{j} = \rho\mathbf{u} = \sum_{\alpha=1}^{8} e_\alpha f_\alpha \tag{9}$$

In addition, in Eq. (1), the equilibrium moments are:

$$e^{eq} = -2\rho + 3\left(j_x^2 + j_y^2\right)/\rho,\ \varepsilon^{eq} = \rho - 3\left(j_x^2 + j_y^2\right)/\rho \tag{10}$$

$$q_x^{eq} = -j_x, q_y^{eq} = -j_y \tag{11}$$

$$p_{xx}^{eq} = (j_x^2 - j_y^2)/\rho, p_{xy}^{eq} = j_x j_y/\rho \tag{12}$$

The transform matrix is given by [19]:

$$M = \begin{bmatrix} 1 & 1 & 1 & 1 & 1 & 1 & 1 & 1 & 1 \\ -4 & -1 & -1 & -1 & -1 & 2 & 2 & 2 & 2 \\ 4 & -2 & -2 & -2 & -2 & 1 & 1 & 1 & 1 \\ 0 & 1 & 0 & -1 & 0 & 1 & -1 & -1 & 1 \\ 0 & -2 & 0 & 2 & 0 & 1 & -1 & -1 & 1 \\ 0 & 0 & 1 & 0 & -1 & 1 & 1 & -1 & -1 \\ 0 & 0 & -2 & 0 & 2 & 1 & 1 & -1 & -1 \\ 0 & 1 & -1 & 1 & -1 & 0 & 0 & 0 & 0 \\ 0 & 0 & 0 & 0 & 0 & 1 & -1 & 1 & -1 \end{bmatrix} \tag{13}$$

This matrix maps the distribution functions to their moments in the following form:

$$\mathbf{m} = M\cdot\mathbf{f},\ \ \mathbf{f} = M^{-1}\cdot\mathbf{m} \tag{14}$$

The diagonal matrix $\widehat{S}$ of relaxation rates $\{s_i\}$ is given by:

$$\widehat{S} = \text{diag}(0, s_1, s_2, 0, s_4, 0, s_6, s_7, s_8) \tag{15}$$

Where the relaxation rates $s_7 = s_8 = 1/\tau$ determines the dimensionless viscosity of the model:

$$\nu = \left(\tau - \frac{1}{2}\right)c_s^2\delta t \tag{16}$$

The speed of sound in D_2Q_9 model is $c_s = c/\sqrt{3}$. Pressure and density are related to each other by the equation of state for an ideal gas, $P = \rho c_s^2$. Other relaxation rates s_1,s_2 and $s_4 = s_6 = s_q$ are usually indicated by linear stability of the model [19]. In addition, the no-slip boundary conditions will also determine the choice of $s_4 = s_6$ [15].

With the above equilibrium moments, if all relaxation rates are set to be a single value $1/\tau$, i.e., $\widehat{S} = \tau^{-1}I$, where I is 9×9 identity matrix, then the model is equivalent to an LBGK model with the following equilibrium distribution function:

$$f_\alpha^{(eq)} = \rho w_\alpha\left[1 + \frac{3}{c^2}e_\alpha\cdot u + \frac{9}{2c^4}(e_\alpha\cdot u)^2 - \frac{3}{2c^2}u\cdot u\right] \tag{17}$$

For D_2Q_9 model, the coefficients $w_0 = 4/9$, $w_\alpha = 1/9$ for $\alpha = 1$–4, and $w_\alpha = 1/36$ for $\alpha = 5$–8.

2.2. Method of solution and boundary conditions

Flow in porous media usually involves three scales: the pore scale, the representative elementary volume (REV) scale and the domain scale. In classical studies, flow in porous media is usually modeled by some semi-empirical models due to the complex structure of a porous medium, based on volume averaging at the REV scale [14]. Moreover, several models such as Darcy, Brinkman-extended Darcy and the Forchheimer-extended Darcy have also been used to simulate flow through porous media. Usually, two approaches have been used in lattice Boltzmann simulation of fluid flow in porous media: the pore scale approach and the REV approach. In the pore level approach, the fluid between the pores of the medium is modeled directly by the standard lattice Boltzmann equation (LBE), and the interaction between the fluid and solid is modeled by the no-slip bounce-back rule. In the REV approach, the standard LBE is modified by including an additional term to account due to the presence of the porous medium. The pore scale approach is the most straightforward way to apply the LBM to porous flows. In this study, simulation of fluid flow in two-dimensional random porous media at pore level is examined. The first matter in this analysis is to determine the structure of the porous medium. Since, there is not any regular distribution of particles in actual porous media; a random generator is used to produce the porous medium. Two-dimensional square obstacles are randomly and with free overlapping distributed between two parallel plates. The random generator must distribute solid obstacles in the domain uniformly, such that its porous generation differs, when it runs at different times. A void fraction function $F(x)$ is used to differentiate solid nodes from fluid nodes, such that

$$F(x) = \begin{cases} 0 & \text{fluid} \\ 1 & \text{solid} \end{cases} \tag{18}$$

The total volume of filled cells must produce the desired porosity. The Boundary conditions for the simulation are specific velocity and pressure at the inlet and outlet sections, respectively, and no-slip boundary condition at solid-fluid interactions (upper and lower walls, and solid-fluid boundaries in the interior domain). Since, in the lattice Boltzmann simulations, the unknowns are distribution functions, therefore, these boundary conditions should be represented in the distribution functions.

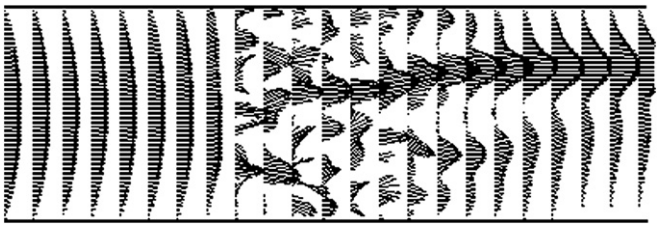

Fig. 2. Velocity vectors in a duct including porous segment, $Re_{Lx} = 450$.

At the inlet and outlet sections of the domain, the method proposed by Lim et al. [20] is used to demonstrate the given boundary conditions in terms of the distribution functions as follows:

$$\left.\begin{aligned} f_1(x=0,y,t) &= f_1^{eq}(\rho, u=u_{\text{inlet}}, v=0, x=0, y, t) \\ f_5(x=0,y,t) &= f_5^{eq}(\rho, u=u_{\text{inlet}}, v=0, x=0, y, t) \\ f_8(x=0,y,t) &= f_8^{eq}(\rho, u=u_{\text{inlet}}, v=0, x=0, y, t) \end{aligned}\right\} \text{at inlet} \tag{19}$$

$$\left.\begin{aligned} f_3(LX,y,t) &= f_3^{eq}(\rho_{\text{out}}, u, v, x=LX, y, t) \\ f_6(LX,y,t) &= f_6^{eq}(\rho_{\text{out}}, u, v, x=LX, y, t) \\ f_7(LX,y,t) &= f_7^{eq}(\rho_{\text{out}}, u, v, x=LX, y, t) \end{aligned}\right\} \text{at outlet} \tag{20}$$

In Eq. (19), the values of u,v are given due to the specific velocity boundary condition at the inlet and the density values are extrapolated from the flow domain whereas in Eq. (20), the values of density are given owing to the equation of state, and the u and v values are obtained using a second order extrapolation from the interior domain.

The bounce-back boundary condition is used at lower and upper walls and the solid-fluid interaction in the interior domain:

$$f_{\bar{\alpha}}(x_f, t+\delta t) = f_{\alpha}(x_f, t) \tag{21}$$

Where x_f is the fluid node next to the boundary location x_b and $e_{\alpha} = -e_{\bar{\alpha}}$. It was shown that the no-slip boundary location is precisely on half lattice spacing beyond the last flow node if the following relation is satisfied [15]:

$$s_q = 8\frac{(2-s_v)}{(8-s_v)} \tag{22}$$

In which $s_v = s_7 = s_8 = 1/\tau$ determines the shear viscosity and $s_4 = s_6 = s_q$ is the relaxation rate for q_x and q_y. It is obvious that the single-relaxation time collision model cannot satisfy this condition.

These boundary conditions with the evolution equation (Eq. (1)) are used to simulate fluid flow in the desired medium.

2.3. Numerical results and verifying the fluid flow computations

The main results of the fluid flow simulation are presented in this section. Channel dimensions were chosen 0.09 × 0.03 m^2 (lenght × height) and obstacle size (d_p) is 0.4 mm. Porosity is assumed to be 0.9 in this study. Calculations were performed using 900 × 300 lattice nodes for $Re_{Lx} = 450$. A typical simulated flow is shown in Fig. 2. The zoomed observation of the velocity field and streamlines in the porous medium are also shown in Fig. 3.a-b to demonstrate the effect of obstacles on the fluid flow.

The validation of computational results of fluid flow in the porous medium is carried out by comparing the pressure drop along the porous medium with the results of other researchers. The non-dimensional pressure gradient ($-dP/dX$) in the porous medium versus Re_{dp} for $\phi = 0.9$ is shown in Fig. 4. In order to calculate ($-dP/dX$), the non-dimensional pressure difference between the inlet and outlet of the porous matrix is divided by its non-dimensional length. The inlet and outlet fluid pressures are determined using the following equation:

$$P = \frac{\sum_{j=1}^{j\max} P_j}{j\max} \tag{23}$$

For validation of the pressure drop, Darcy law with Forchheimer term is used which are as follows [21–24]:

$$-\nabla\tilde{P} = \frac{\mu}{\kappa}u_{g_0} + A\cdot\rho u_{g_0}^2 \tag{24}$$

Where parameter A in Eq. (24) is an empirical function given by:

$$A = \frac{1.75(1-\phi)}{\phi^3 d_p} \tag{25}$$

To determine the permeability κ, the two following forms are used:

$$k = \frac{\phi^3 d_p^2}{150(1-\phi)^2} \tag{26}$$

$$k = \frac{\phi^3 d_p^2}{175(1-\phi)^2} \tag{27}$$

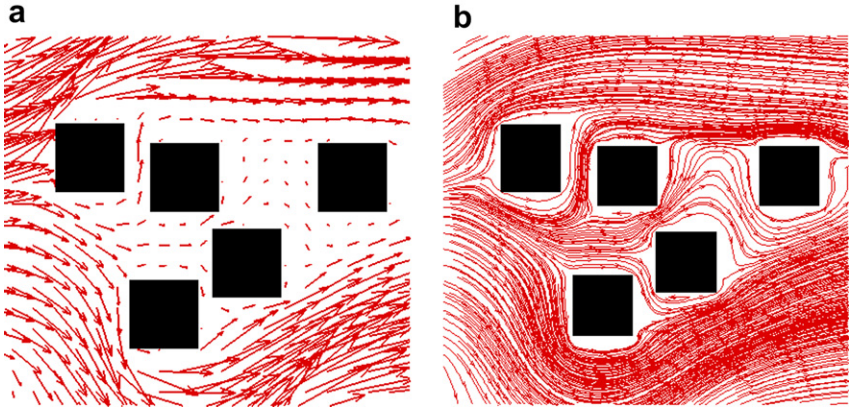

Fig. 3. (a) Vector field inside the porous medium, (b) streamlines inside the porous medium, $\phi = 0.9$.

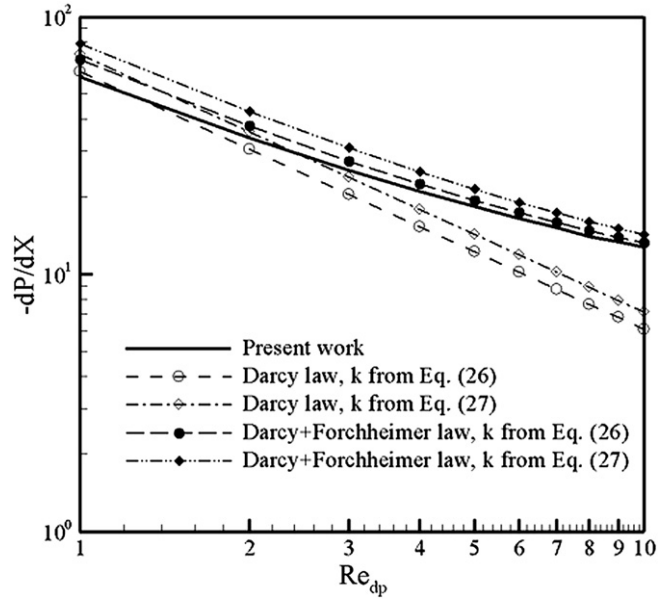

Fig. 4. Variation of non-dimensional pressure drop with Re_{dp} along porous medium ($\phi = 0.9$).

It should be noted that the relations 25–27 are empirical relations to model the permeability k and the parameter A for porous media of spheres. However, it was not found any special equations for porous media of square cylinders in the literatures. Besides, these relations were employed for the similar configuration in Ref. [21].

As Fig. 4 shows, there is nearly a good agreement between the pressure drop that is calculated in the present analysis and those calculated based on Eq. (24).

Morover, to investigate the grid dependency of the results, three different sizes of domain and obstacles were used: 4 × 4 obstacles in a 360 × 120 domain, 5 × 5 obstacles in a 450 × 150 domain and 6 × 6 obstacles in a 540 × 180 domain. The non-dimensional pressure gradients for these three grids are summarized in Table 1. The difference between second and third grid is below 1% therefore, we use the second one to validate our results. In addition, we created 12 media with different random obstacle placement for 450 × 150 domain and the Reynolds number of 450. The mean non-dimensional pressure gradient and standard deviation for these media are shown in the Table 2. The comparison between the non-dimensional pressure gradient for the random and uniform porous medium in Table 1 and the mean non-dimensional pressure gradient for these media shows relatively good agreement.

3. Thermal analysis

3.1. Detailed description of the problem

When a high temperature gas of T_{g0} flows through a duct wherein a porous medium with extremely high porosity is positioned, a large temperature drop ΔT occurs along the porous medium and large amount of converted radiant energy $\bar{q}_{\mathrm{rad}}(0)$ propagates to upstream direction of the gas flow.

Table 1
The non-dimensional pressure gradient for different grids.

Grid	Obstacle	Non-dimensional pressure gradient
360 × 120	4 × 4	17.9890
450 × 150	5 × 5	16.5135
540 × 180	6 × 6	16.4015

Table 2
Mean non-dimensional pressure gradient and standard deviation for different media.

Porosity	Mean non-dimensional pressure gradient	Standard deviation (%)
0.9	17.5418	6.47

Problem under consideration is schematically depicted in Fig. 5. A random porous medium of length L_x and height L_y is located between two parallel plates. Dimensions of both plates and porous medium in normal direction to the gas flow are remarkably large to ensure the two dimensionality of the problem. The high temperature gas of T_{g0} enters the duct at $x = -x_i$. Fluid flow is laminar and steady and lattice Boltzmann method was used before to simulate the flow in random porous medium. The porous segment is assumed to be gray, emitting, absorbing and isotropically scattering. The high temperature gas is presumed to be non-radiative. Incoming radiative fluxes from the upstream and downstream sides towards the porous layer are B_1 and B_2, respectively. Since, the gas and solid phases are in non-local thermal equilibrium, separate energy equations for both solid and gas phases must be considered. All thermophysical properties of both phases and radiative properties of solid phase are assumed to be constant.

3.2. Governing equations and boundary conditions

As mentioned before, because of the non-local thermal equilibrium between solid and gas phases, two separate energy equations for both phases are considered. Therefore, the governing equations are energy equation for gas flow and porous medium and radiative transfer equation for solid phase. To save space, only the non-dimensional forms of the governing equations are presented here:

Non-dimensional gas energy equation:

$$\frac{\phi}{Pe}\left(\frac{\partial^2\theta_g}{\partial\eta_x^2}+\frac{\partial^2\theta_g}{\partial\eta_y^2}\right)-\left(\overline{U}\frac{\partial\theta_g}{\partial\eta_x}+\overline{V}\frac{\partial\theta_g}{\partial\eta_y}\right)-P_1(\theta_g-\theta_p)=0 \tag{28}$$

Non-dimensional solid energy equation:

$$(1-\phi)P_2\left(\frac{\partial^2\theta_p}{\partial\eta_x^2}+\frac{\partial^2\theta_p}{\partial\eta_y^2}\right)-\overset{*}{\nabla}\cdot Q_{\mathrm{rad}}+P_3(\theta_g-\theta_p)=0 \tag{29}$$

All of the non-dimensional parameters used in Eqs. (28), (29) are given in the Nomenclature. Two energy equations are coupled through the convective heat transfer between solid and gas phases. It should be noted that by considering the convection coefficient between gas and solid phases, the energy equations are written by integral method, but for a differential control volume of $(dx \times dy)$ that comprises a number of solid particles based on the medium porosity. Therefore, the method which is employed for obtaining

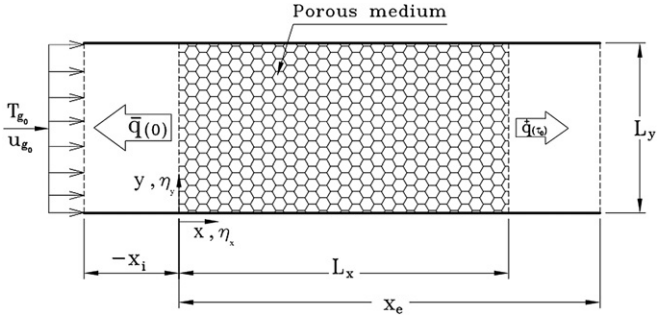

Fig. 5. Schematic diagram of a heat recovery system.

the gas and solid energy equations may be called as integral-differential one. Besides, the value of convection coefficient is evaluated by empirical correlation given in Ref [25].

In Eq. (29), $\overset{*}{\nabla}\cdot Q_{rad}$ is the non-dimensional divergence of radiative heat flux that should be calculated from the radiative transfer equation and can be written in the following form:

$$\overset{*}{\nabla}\cdot Q_{rad} = \left(\frac{\partial Q_x}{\partial \eta_x}+\frac{\partial Q_y}{\partial \eta_y}\right) \tag{30}$$

The general equation of radiative transfer for an absorbing, emitting and anisotropically scattering medium is written in dimensionless form as follows [26]:

$$\hat{s}\cdot\overset{*}{\nabla} I^*(\vec{r},\hat{s}) = -\tau_0 I^*(\vec{r},\hat{s})+\tau_1 I_b^*(\vec{r}) + \frac{\tau_2}{4\pi}\int_{\omega'=4\pi} I^*(\vec{r},\hat{s}')\varphi(\vec{r},\hat{s},\hat{s}')d\Omega' \tag{31}$$

Eq. (31) is valid for a gray medium or, on a spectral basis, for a non-gray medium. Once the intensities have been determined from Eq. (31), the radiative heat flux inside the medium may be found from Eq. (32):

$$Q_{rad}(\vec{r}) = \int_{4\pi} I^*(\vec{r},\hat{s})\hat{s}d\Omega \tag{32}$$

To solve the gas energy equation, the following boundary conditions are used:

$$\theta_g = 1 \quad \text{at } \eta_x = 0 \tag{33}$$

$$\frac{\partial\theta_g}{\partial\eta_x} = Nu(\theta_p-\theta_g) \quad \text{at } \eta_x = 1 \tag{34}$$

$$\frac{\partial\theta_g}{\partial\eta_y} = P_5(\theta_g-\theta_\infty) \quad \text{at } \eta_y = 0 \tag{35}$$

$$\frac{\partial\theta_g}{\partial\eta_y} = -P_5(\theta_g-\theta_\infty) \quad \text{at } \eta_y = \eta_{Ly} \tag{36}$$

Eq. (34) represents heat transfer between gas and solid phases at the exit section of the porous matrix, which includes conduction heat transfer of the gas phase (the partial derivative term) and energy transfer between gas and solid phases by convection.

For the solid phase at locations $\eta_x = 0$ and 1, where heat transfer between the gas and solid phase is by convection and heat transfer between porous matrix and its surrounding is by radiation, following boundary conditions are employed:

$$Bi(1-\theta_{p_0})+\frac{\varepsilon_{p_i}}{P_2}\left(\theta_i^4-\theta_{p_0}^4\right) = -\frac{\partial\theta_p}{\partial\eta_x} \quad \text{at } \eta_x = 0 \tag{37}$$

$$Bi(\theta_{p_L}-\theta_{g_L})+\frac{\varepsilon_{p_e}}{P_2}\left(\theta_{p_L}^4-\theta_e^4\right) = -\frac{\partial\theta_p}{\partial\eta_x} \quad \text{at } \eta_x = 1 \tag{38}$$

On the upper and lower walls, the following boundary conditions are considered:

$$\frac{\partial\theta_p}{\partial\eta_y} = P_4(\theta_p-\theta_\infty) \quad \text{at } \eta_y = 0 \tag{39}$$

$$\frac{\partial\theta_p}{\partial\eta_y} = -P_4(\theta_p-\theta_\infty) \quad \text{at } \eta_y = \eta_{Ly} \tag{40}$$

Partial derivative term that is used in Eqs. (34)–(40) shows the conduction heat transfer of gas and solid phases. In addition, Eqs. (35), (36), (39) and (40) show heat transfer between the gas and solid phases with the environment at lower and upper walls, respectively.

To solve the radiative transfer equation, appropriate boundary conditions are needed. It is assumed that incoming radiations B_1 and B_2 are applied to the system from the inlet and outlet sections of the porous medium, respectively. Therefore, the radiative boundary conditions at the four boundaries are as follows:

$$I^{*m}(0,\eta_y) = \frac{B_1'}{\pi} \quad \text{at } \eta_x = 0 \tag{41}$$

$$I^{*m}(1,\eta_y) = \frac{B_2'}{\pi} \quad \text{at } \eta_x = 1 \tag{42}$$

$$I^{*m}(\eta_x,0) = \varepsilon_B\frac{\sigma\theta_B^4}{\pi}+\frac{\rho_B}{\pi}\int_{\hat{n}\cdot\hat{s}'<0}|\hat{n}\cdot\hat{s}'|\,I^*(\eta_x,0,\hat{s}')d\Omega' \quad \text{at } \eta_y = 0 \tag{43}$$

$$I^{*m}(\eta_x,\eta_{L_y}) = \varepsilon_T\frac{\sigma\theta_T^4}{\pi}+\frac{\rho_T}{\pi}\int_{\hat{n}\cdot\hat{s}'<0}|\hat{n}\cdot\hat{s}'|I^*(\eta_x,\eta_{L_y},\hat{s}')d\Omega' \quad \text{at } \eta_y = \eta_{L_y} \tag{44}$$

3.3. Discrete ordinates method (S_N approximation)

One of the methods that are commonly used to solve the radiative transfer equation (RTE) is the discrete ordinates method (DOM). The DOM is based on a discrete representation of the directional variation of the radiative intensity. Most of credit in our opinion for the introduction and development of DOM go to Chandrasekhar [26], who used this method in his fundamental work on radiative transfer equation. Today, DOM is a well known technique to solve the RTE such that the details of this method are completely described in Ref. [27]. This method transforms the equation of transfer into a set of simultaneous partial differential equations. The name S_N approximation indicates that N different direction cosines are used for each principal direction. Altogether, there are $n = N(N+2)$ different directions to be considered, for radiant intensities. A solution to the transport problem is found by solving the equation of transfer for a set of discrete directions spanning the total solid angle range of4π. Integrals over solid angle are approximated by numerical quadrature. Using the discrete ordinates method, the general equation of transfer (Eq. (31)) is solved for a set of n different directions $\hat{s}_i$, $i = 1, 2, \ldots, n$, such that the integrals over direction are replaced by quadratures as follows:

$$\int_{4\pi} f(\hat{s})d\Omega \approx \sum_{i=1}^{n} w_i f(\hat{s}_i) \tag{45}$$

Where the w_i are the quadrature weights associated with the directions $\hat{s}_i$. In this way, Eq. (31) is approximated by a set of n differential equations as follows:

$$\hat{s}_i\cdot\overset{*}{\nabla} I^*(\vec{r},\hat{s}_i) = -\tau_0 I^*(\vec{r},\hat{s}_i)+\tau_1 I_b^*(\vec{r}) + \frac{\tau_2}{4\pi}\sum_{j=1}^{n} w_j I^*(\vec{r},\hat{s}_j)\varphi(\vec{r},\hat{s}_i,\hat{s}_j) \quad i = 1,2,\ldots,n \tag{46}$$

Once the intensities have been determined in the desired directions, integrated quantities can be readily calculated. Then, the radiative flux method inside the medium may be found from:

$$Q_{\mathrm{rad}}(\vec{r}) = \int_{4\pi} I^*\left(\vec{r},\hat{s}_i\right)\hat{s}_i d\Omega \approx \sum_{i=1}^{n} w_i I_i^*(\vec{r})\hat{s}_i \tag{47}$$

For the two-dimensional Cartesian coordinates system, Eq. (46) becomes

$$\xi^m \frac{\partial I^{*m}}{\partial \eta_x} + \eta^m \frac{\partial I^{*m}}{\partial \eta_y} = -\tau_0 I^{*m} + \tau_1 I_b^* + \frac{\tau_2}{4\pi}\sum_{m'} w^{m'}\varphi^{m'm} I^{*m'} \tag{48}$$

Where m,m' denote outgoing and incoming directions, respectively.

The finite difference form of Eq. (48) gives the following form for radiant intensity:

$$I_{i,j}^{*m} = \frac{IX^m + IY^m + \tau_1 I_{b,i,j}^* + S^{*m}}{\tau_0 + X^m \mathrm{Sign}(X^m) + Y^m \mathrm{Sign}(Y^m)} \tag{49}$$

Where

$$IX^m = X^m u_0(X^m) I_{i-1,j}^{*m} - X^m u_0(-X^m) I_{i+1,j}^{*m}$$

$$IY^m = Y^m u_0(Y^m) I_{i,j-1}^{*m} - Y^m u_0(-Y^m) I_{i,j+1}^{*m}$$

$$X^m = \frac{\xi^m}{\Delta\eta_x}$$

$$Y^m = \frac{\eta^m}{\Delta\eta_y}$$

$$S^{*m} = \frac{\tau_2}{4\pi}\sum_{m'} w^{m'}\varphi^{m'm} I_{i,j}^{*m'}$$

$$u_0(x) = \begin{cases} 1 & x > 0 \\ 0 & x < 0 \end{cases}$$

$$\mathrm{Sign}(x) = \begin{cases} 1 & x > 0 \\ -1 & x < 0 \end{cases}$$

The details of numerical solution of RTE by DOM were also described in the previous work by the second author in which the thermal characteristics of porous radiant burner were investigated [28].

3.4. Solution strategy

In the thermal analysis of the heat recovery system, to determine the values of dependent variables θ_g, θ_p and Q_{rad} at each nodal point in the 2-D computational domain, the couple equations (28), (29) and (31) should be solved simultaneously.

The numerical solution of Eq. (48) can be started with the black body assumption for the boundaries with neglecting the source termS^*. In the next iterations, the general form of Eq. (49) and its boundary conditions are applied. This procedure is repeated until the convergence criterion is met. Finally, from the radiative intensities obtained by Eq. (49), the divergence of the radiative heat flux can be calculated from the following equation:

$$\overset{*}{\nabla}\cdot Q_{\mathrm{rad}} = 4\pi\tau_1\left(I_b^* - \frac{1}{4\pi}\sum_{m'} w^{m'} I^{*m'}\right) \tag{50}$$

For solving the gas energy equation (Eq. (28)), u- and v- velocity components at each nodal point through the porous medium are needed. These values are obtained using the lattice Boltzmann method. As mentioned in Section 3.2, the energy equations are written by integral method, but for a differential control volume of $(dx \times dy)$ that comprises a number of solid particles based on the medium porosity. Considering this point, each control volume contains some pore and void nodes. Velocity values at these nodes are obtained using LBM and then by averaging between the velocities of these nodes at each control volume (volume-averaged velocity), one can obtain the velocities that are used in gas energy equation. It should be noted that gas and solid energy equations along with radiative transfer equation are solved after the time-independent velocity are obtained by the lattice Boltzmann method.

Finite difference forms of the gas and solid energy equations are obtained using central differencing for derivative terms where the error of discretization is the order of $(\Delta\eta_x^2)$ and $(\Delta\eta_y^2)$. For obtaining the grid independent solution, a uniform grid of 80 × 60 nodal points in the computational domain is used.

The sequence of calculations can be stated as follows:

1. A first approximation of each dependent variable θ_g and θ_p is assumed.
2. S_6 approximation is used to solve the radiative transfer equation to obtain the values of I^*, Q_{rad} and $\nabla\cdot Q_{\mathrm{rad}}$ at each nodal point.
3. Using the values of $\nabla\cdot Q_{\mathrm{rad}}$, the solid energy equation is solved and the values of θ_p are calculated.
4. The values of θ_g are computed by numerical solution of the gas energy equation.
5. Steps 2–4 are repeated until convergence is obtained. This condition was assumed to have been achieved when the fractional changes in the temperature and radiative intensity between the two consecutive iteration levels did not exceed 10^{-6} at each nodal point.

4. Validation of the computational results

Since, we could not find any theoretical or experimental results for such a two-heat recovery system in literatures, the present numerical results are compared with theoretical predictions in Ref. [29] about a 2-D porous radiant burner. It should be noted that the non-dimensional form of the governing equations for the porous radiant burner are the same as used for the heat recovery system, except that an additional term $\phi P_6\delta(\eta_x)$ that accounts for the heat generation term $(\dot{Q})$ in the combustion zone of the radiant burner must be added where P_6 and $\delta(\eta_x)$ are as follows:

$$P_6 = \frac{\dot{Q}L_x}{T_{g_0}\rho_g u_g c_g}$$

$$\delta(\eta_x) = \begin{cases} 1 & 0.5 < \eta_x < 0.5 + \Delta x_{\mathrm{flame}}/L_x \\ 0 & \text{elsewhere} \end{cases}$$

For the test case under consideration, $L_x = 0.1\ m$, $L_y = 0.1\ m$ and the thickness of the heat generation zone $(\Delta x_{\mathrm{flame}})$ was set to 0.01 m. The non-dimensional parameters for this test case are given in Table 3 [29]. The gas temperature distributions along the burner at the mid-plane $(\eta_y = 0.5)$ are presented in Fig. 6. It is seen that the incoming air-fuel mixture is preheated by radiation in the region upstream to the combustion zone. The maximum temperature takes place inside the heat generation domain after which the gas temperature decreases by converting gas enthalpy to thermal

Table 3
Non-dimensional parameters of the test case from Talukdar et al. [29].

Parameter	Value
P_1	102.80
P_2	666.45
P_3	3.33×10^4
P_4	0.00
P_5	0.00
P_6	103.48
Pe	38.91
Nu	400.00
Bi	5.00
B'_1	1.00
B'_2	1.00
β	0.00

Table 4
Non-dimensional parameters of the present heat recovery system [29].

Parameter	Value
P_1	2.73×10^6
P_2	5.88
P_3	10.23×10^6
P_4	0.00
P_5	0.00
Pe	88.34
Nu	2074.69
Bi	15.00
B'_1	0.00
B'_2	0.00

radiation. However, Fig. 6 shows a good agreement between the present results and those obtained theoretically in Ref. [29].

5. Results and discussion

The thermal behavior of a heat recovery system which works based on the energy conversion between gas enthalpy and thermal radiation are analyzed here. In the 2-D rectangular heat recovery system considered in this study, there are many independent parameters, but it is possible to present only some results for a wide range of conditions. Table 4 [29] shows the non-dimensional parameters that are used in this study. The porous medium is considered non-scattering, except in Figs. 10 and 11 in which the effect of scattering is considered. It should be noted that the values of aspect ratio $r = L_x/L_y$ is always kept to 1. The temperature of working gas at the inlet section of the porous matrix is equal to 1000 K.

The variations of θ_g, θ_p along the porous matrix at centerline ($\eta_y = 0.5$) are shown in Fig. 7 for two different values of the optical thickness τ_0. There is a considerable temperature drop in the gas flow, especially at the entrance of the porous matrix. This characteristic constitutes the basic principle to support an effective energy conversion from gas enthalpy to thermal radiation. The sharp gas temperature drop at the entrance region of the porous segment causes to have a considerable amount of the recaptured radiative flux from the porous media ($Q^-_{rad}(0)$) towards the upstream direction (into the thermal system). It should be noted that it is desirable to have a large amount of radiation emitted from the porous segment in the upstream direction to minimize the energy that may otherwise be wasted. Further, it is worth having a close look at the small temperature difference between gas and porous temperatures which is due to the large convection heat transfer coefficient. This figure also shows that the higher optical thickness results in more decrease in the temperature of working gas.

In Fig. 8 the variations of radiative fluxes Q^+_{rad} and Q^-_{rad} along the layer and at the mid-plane ($\eta_y = 0.5$) are presented for the optical thickness of $\tau_0 = 2$. The radiative heat flux Q^-_{rad} has its maximum value at the entrance of the porous layer. It is a useful behavior of this recovery system because $Q^-_{rad}(0)$ is the recovered radiative energy.

Isotherm lines for the two-dimensional porous media under consideration are shown in Fig. 9. This figure shows that there is not any considerable variation of gas temperature along the y-axis. Besides, the non-regular curvature of the isotherms is due to the

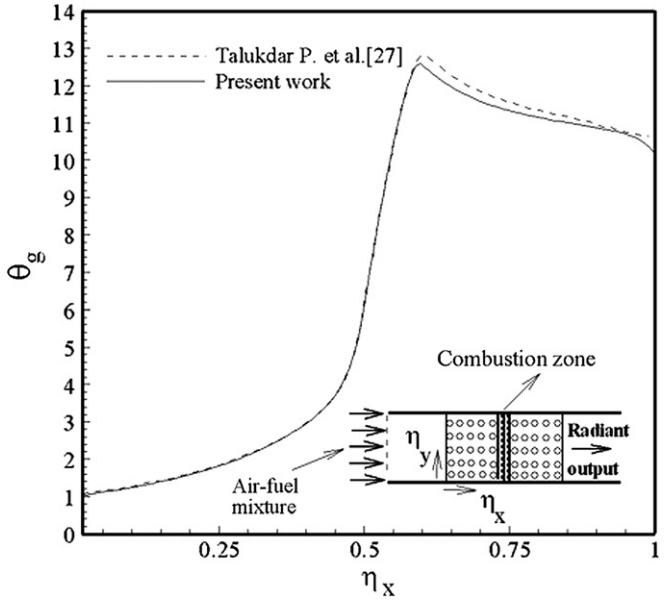

Fig. 6. Gas temperature distribution along the porous radiant burner with uniform heat generation.

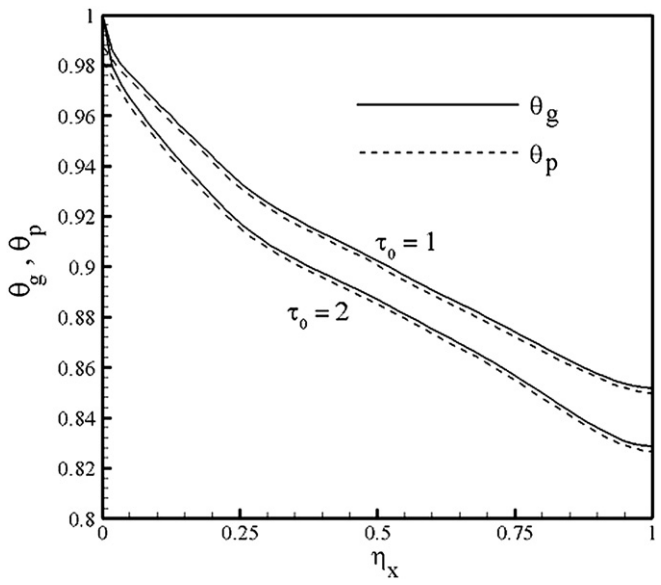

Fig. 7. Distribution of gas and solid temperatures along the porous matrix at the mid-plane ($\eta_y = 0.5$), $\omega = 0.00$.

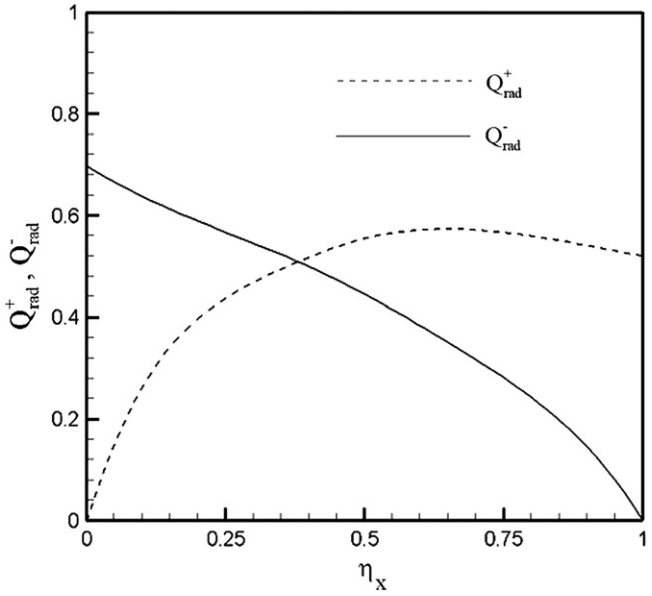

Fig. 8. Variation of radiative heat flux inside the porous medium at the mid-plane ($\eta_y = 0.5$), $\omega = 0.00$, $\tau_0 = 2.00$.

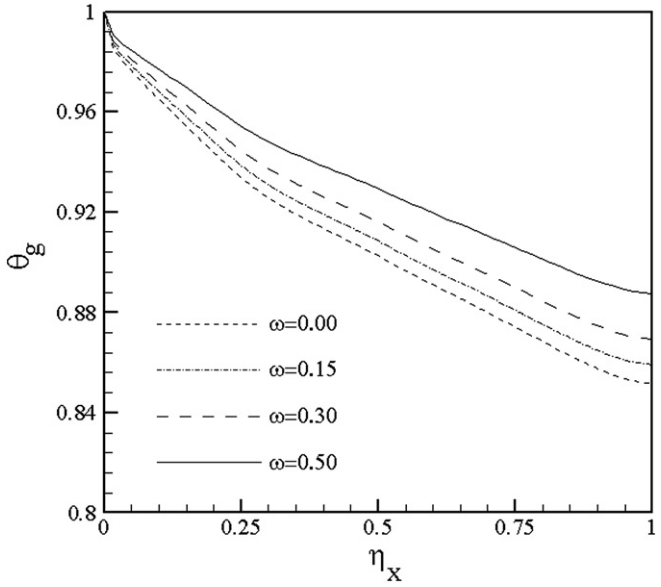

Fig. 10. The effect of scattering albedo on gas temperature drop through the porous matrix, ($\eta_y = 0.5$), $\tau_0 = 1.00$.

random variation of gas velocity according to the random existence of solid particles in different locations. Also, the gas temperature drop along the flow direction can easily be seen through the porous segment.

To study the effect of scattering albedo (ω) on the energy conversion from gas enthalpy to thermal radiation, the gas temperature drop across the porous layer as a function of ω is shown in Fig. 10. It can be seen that values of enthalpy drop decrease with increasing ω. For further study of the effect of thermal scattering on the performance of the heat recovery system, the variations of $Q^+_{rad}(\eta_x = 1)$ and $Q^-_{rad}(\eta_x = 0)$ with scattering albedo are presented in Fig. 11. It should be mentioned that $Q^+_{rad}(\eta_x = 1)$ and $Q^-_{rad}(\eta_x = 0)$ are the outgoing radiative fluxes from two ends of the porous segment, one to the downstream and the other to the upstream directions. It is seen from Fig. 11 that, the higher value of scattering albedo causes a decrease in the value of $Q^-_{rad}(\eta_x = 0)$. Therefore, it can be concluded that the porous layers with low scattering coefficients are suitable for this energy conversion such that the maximum values of temperature drop are obtained by using non-scattering media ($\omega = 0$).

As mentioned before, the porous media that emit more backward radiative flux $Q^-_{rad}(\eta_x = 0)$ are more efficient for heat recovery purpose; this action can be achieved when the porous layers with high optical thickness are used as it is seen in Fig. 12.

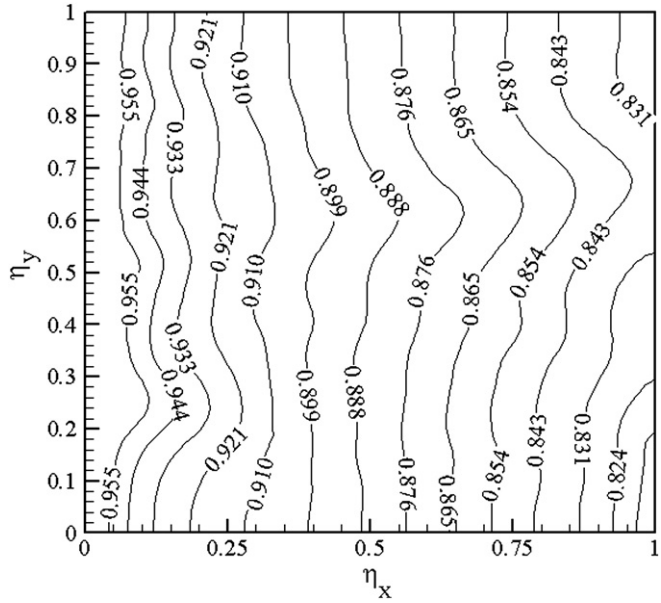

Fig. 9. Contours of gas temperature in the 2-D heat recovery system, $\omega = 0.00$, $\tau_0 = 2.00$.

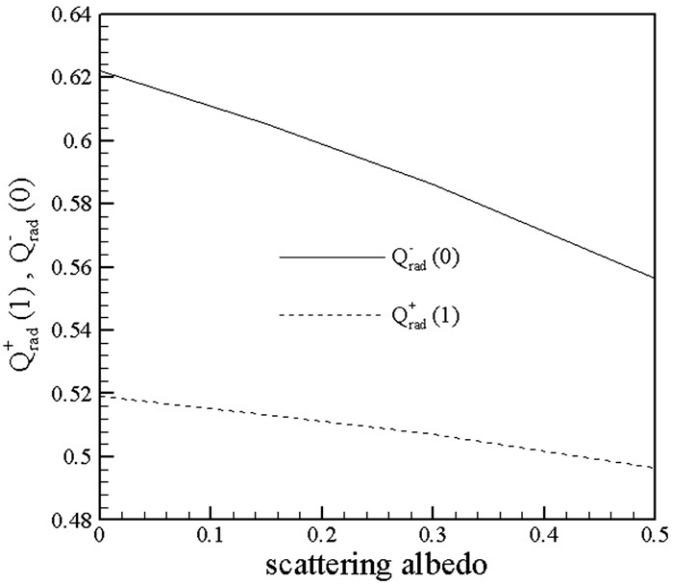

Fig. 11. Variation of radiative heat flux at the inlet and outlet sections of the porous segment with scattering albedo, ($\eta_y = 0.5$), $\tau_0 = 1.00$.

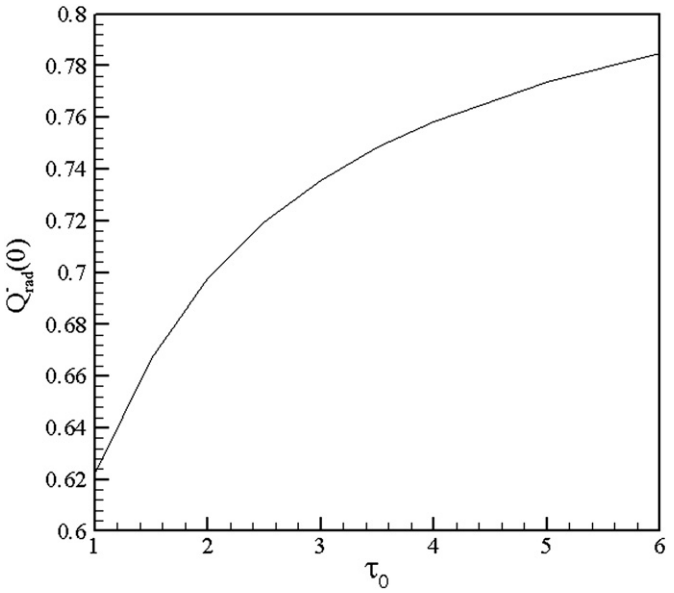

Fig. 12. The effect of optical thickness on the radiative heat flux at the inlet of the porous medium $\omega = 0.00$.

6. Conclusions

A numerical study has been fulfilled to explore the fluid and thermal behaviors of a two-dimensional porous heat recovery system. Lattice Boltzmann method was applied to simulate fluid flow in the porous medium and the effect of obstacles on the flow field were considered. Since, gas and solid phases are not in local thermal equilibrium, two separate energy equations were considered for these phases. Gas phase was assumed to be non-radiative whereas solid phase can absorb, emit and scatter thermal radiation. Discrete ordinates method was employed to solve the radiative transfer equation for computing the radiative heat flux distribution in the porous medium. The efficiency of the porous heat recovery system depends on the recovered radiative energy. To this end, the effect of optical thickness and scattering albedo on the performance of the heat recovery system was examined. It was found that the amount of the recaptured radiative flux from inlet section of the porous medium towards the upstream direction increases by choosing the porous medium with higher optical thickness. Furthermore, the higher value of scattering albedo makes a decrease in the value of recovered radiative energy. It can be concluded that porous layers with high optical thickness and low scattering albedo are more efficient in recovering heat from high temperature gases.

References

[1] R. Echigo, Effective energy conversion method between gas enthalpy and thermal radiation and application to industrial furnaces, in: Proc. 7th Int. Heat Transfer Conf., München, vol. 6, 1982, pp. 361–366.
[2] Y. Yoshizawa, R. Echigo, T.A. Tomimura, Study on a high performance radiant heater, in: Proc. Of 1987 ASME-JSME thermal Engineering Joint Conf., Honolula, 1983, vol. IV, pp. 99–103.
[3] S.B. Sathe, T.W. Tong, A numerical analysis of heat transfer and combustion in porous radiant burners. Int. J. Heat Mass Transfer 33 (1990) 1331–1338.
[4] K.Y. Wang, C.L. Tien, Thermal insulation in flow systems combined radiation and convection through a porous segment. J. Heat Transfer 106 (1984) 453–459.
[5] H. Yoshida, J.H. Yun, R. Echigo, T. Tomimura, Transient characteristics of combined conduction, convection and radiation heat transfer in porous media. Int. J. Heat Mass Transfer 33 (5) (1990) 847–857.
[6] S.A. Gandjalikhan Nassab, Transient characteristics of an energy recovery system using a porous medium, in: Proc. Instn. Mech. Engrs., Part A. J. Power and Energy 216, 2002, pp. 387–394.
[7] S.A. Gandjalikhan Nassab, M. Maramisaran, Transient numerical analysis of a multi-layered porous heat exchanger including gas radiation effect. Int. J. Thermal Sci. 48 (2009) 1586–1595.
[8] T. Tomimura, K. Hamano, Y. Honda, R. Echigo, Experimental study on a multi-layered type gas-to-gas heat exchanger using porous media. Int. J. Heat Mass Transfer 47 (2004) 4615–4623.
[9] R. Benzi, S. Succi, M. Vergassola, The lattice Boltzmann equation theory and applications. Phys. Rep. 222 (1992) 145–197.
[10] S. Chen, G.D. Doolen, Lattice Boltzmann method for fluid flows. Annu. Rev. Fluid Mech. 30 (1998) 329–364.
[11] E. Foti, S. Succi, F. Higuera, Three-dimensional flows in complex geometries with the lattice Boltzmann method. Europhysics Lett. 10 (5) (1989) 433–438.
[12] A. Cancelliere, C. Chang, E. Foti, D.H. Rothman, S. Succi, The permeability of a random medium: comparison of simulation with theory. Phys. Fluids A 2 (12) (1990) 2085–2088.
[13] A. Koponen, D. Kandhai, E. Hellén, M. Alava, A. Hoekstra, M. Kataja, K. Niskanen, P. Sloot, J. Timonen, Permeability of three-dimensional random fiber webs. Phys. Rev. Lett. 80 (4) (1998) 716–719.
[14] Z. Guo, T.S. Zhao, Lattice Boltzmann model for incompressible flows through porous media. Phys. Rev. E 66 (3) (2002) id. 036304/1–036304/9.
[15] C. Pan, L.-S. Luo, C.T. Miller, An evaluation of lattice Boltzmann schemes for porous medium flow simulation. Comput. Fluids 35 (8/9) (2006) 898–909.
[16] A. Nabovati, A.C.M. Sousa, Fluid flow simulation in random porous media at pore level using the lattice Boltzmann method. J. Eng. Sci. Tech. 2 (3) (2007) 226–237.
[17] W.W. Yan, Y. Liu, Y.S. Xu, X.L. Yang, Numerical simulation of air flow through a biofilter with heterogeneous porous media. Bioresour. Technol. 99 (7) (2008) 2156–2161.
[18] A. Nabovati, E.W. Llewellin, A.C.M. Sousa, A general model for the permeability of fibrous porous media based on fluid flow simulations using the lattice Boltzmann method. Composites A(40) (2009) 860–869.
[19] P. Lallemand, L.-S. Luo, Theory of the lattice Boltzmann method: dispersion, dissipation, isotropy, Galilean invariance and stability. Phys. Rev. E 61 (6) (2000) 6546–6562.
[20] C.Y. Lim, C. Shu, X.D. Niu, Y.T. Chew, Application of lattice Boltzmann to simulate micro channel flows. Phys. Fluids 14 (7) (2002) 2299–2308.
[21] M.H. Rahimian, A. Pourshaghaghy, Direct simulation of forced convection flow in a parallel plate channel filled with porous media. Int. Comm. Heat Mass Transf. 29 (6) (2002) 867–878.
[22] D. Poulikakos, K. Renken, Forced convection in a channel filled with porous medium, including the effects of flow inertia, variable porosity, and brinkman friction. J. Heat Transf. 109 (4) (1987) 880–888.
[23] K. Renken, D. Poulikakos, Experiment and analysis of forced convective heat transport in a packed bed of spheres. Int. J. Heat Mass Transf. 31 (7) (1988) 1399–1408.
[24] F.C. Chou, W.Y. Lien, Forced convection in a parallel plate channel filled with packed spheres, AIAA/ASME Thermo physics and Heat Transfer Conference, HTD vol. 139, pp. 57–64, ASME, N.Y., 1990.
[25] C. Ben Kheder, B. Cherif, M.S. Sifaoui, Numerical study of transient heat transfer in semitransparent porous medium. Renewable Energy 27 (2002) 543–560.
[26] S. Chandrasekhar, Radiative Transfer. Dover Publications, New York, 1960.
[27] M.F. Modest, Radiative Heat Transfer. McGraw-Hill, New York, 2003.
[28] M.M. Keshtkar, S.A. Gandjalikhan Nassab, Theoretical analysis of porous radiant burners under 2-D radiation field using discrete ordinates method. J. Quant. Spectrosc. Radiat. Transf. 110 (2009) 1894–1907.
[29] P. Talukdar, S.C. Mishra, D. Trimis, F. Durst, Heat transfer characteristics of a porous radiant burner under the influence of a 2-D radiation field. J. Quant. Spectrosc. Radiat. Transf. 84 (2004) 527–537.

Nomenclature

A: surface area per unit volume (m^2/m^3)
$B_{1,2}$: incoming radiations (W/m^2)
$B^{*}_{1,2}$: non-dimensional incoming radiations, $B_{1,2}/\sigma T^4_{g0}$
Bi: Biot number, hL_x/k_p
c_s: sound speed
c_g: specific heat of gas (J/kg °C)
d_p: obstacle size (m)
e: total energy
e_α: discrete particle velocity in LBM
f: density distribution function
F: fraction function
h: convective heat transfer coefficient (W/m^2 °C)
I: intensity (W/m^2)
I^*: non-dimensional intensity, $I/\sigma T^4_{g0}$
j: index of grids in *y* direction
j_{max}: number of grids in *y* direction
j_x: flow momentum in *x* direction
j_y: flow momentum in *y* direction
K_g: gas thermal conductivity (W/m °C)
K_p: solid thermal conductivity (W/m °C)

L_x: length of the porous medium (m)
L_y: height of the porous medium (m)
m: moment
Nu: Nussult number, hL_x/k_g
P: non-dimensional pressure, $\tilde{P}/\rho u_{g_0}^2$
$\tilde{P}$: pressure (pa)
p_{xx}: diagonal component of the stress tensor
p_{xy}: off-diagonal component of the stress tensor
P_1: dimensionless group, $hL_xA/\rho_g c_g u_{g0}(\Delta x \cdot \Delta y)$
P_2: dimensionless group, $K_pL_x/\sigma T_{g0}^3$
P_3: dimensionless group, $hL_xA/\sigma T_{g0}^3(\Delta x \cdot \Delta y)$
P_4: dimensionless group, $h_{wp}L_x/k_p$
P_5: dimensionless group, $h_{wg}L_x/k_g$
Pe: Peclet number, $\rho_g u_{g0} c_g L_x/k_g$
q_{rad}: radiative heat flux (W/m^2)
q_x: heat flux in x direction
q_y: heat flux in y direction
Q_{rad}: dimensionless radiative heat flux, $q_{\mathrm{rad}}/\sigma T_{g0}^4$
r: aspect ratio, L_x/L_y
Re_{Lx}: Reynolds number, $u_{g0}L_x/\upsilon$
Re_{dp}: Reynolds number, $u_{g0}d_p/\upsilon$
$\hat{s}_i$: direction vector in RTE
T: temperature (°C)
T_∞: ambient temperature (°C)
T_{g0}: gas temperature at duct's inlet (°C)
u_g: velocity along x direction (m/s)
u_{g0}: gas velocity at duct's inlet (m/s)
v_g: velocity along y direction (m/s)
$\overline{U}$: non-dimensional x velocity, u/u_{g0}
$\overline{V}$: non-dimensional y velocity, v/u_{g0}
x: coordinate along the flow direction (m)
X: non-dimensional length, L_x/L_y
y: coordinate perpendicular to the flow direction (m)

Greek symbols
α: particle velocity direction
β: extinction coefficient, $\sigma_a + \sigma_s$
∇^*: non-dimensional gradient operator, $L_x\nabla$
Δx: grid spacing along x-axis (m)
Δy: grid spacing along y-axis (m)
$\Delta_{\eta x}$: non-dimensional grid spacing along x-axis, $\Delta x/L_x$
$\Delta_{\eta y}$: non-dimensional grid spacing along y-axis, $\Delta y/L_x$
δt: time step
δx: lattice spacing
ε: energy square
ε: emissivity
η_x: non-dimensional x coordinate, x/L_x
η_y: non-dimensional y coordinate, y/L_x
ν: kinematical viscosity (m^2/s)
ϕ: porosity
φ: scattering phase function
ρ_g: gas density (m^3/kg)
ρ_w: wall reflection coefficient
σ: Stephan-Boltzmann coefficient (w/m^2K^4)
σ_a: absorption coefficient (m^{-1})
σ_s: scattering coefficient (m^{-1})
$\theta_{g,p}$: non-dimensional temperature, $T_{g,p}/T_{g0}$
τ: non-dimensional relaxation time
τ_0: optical thickness, βL_x
τ_1: non-dimensional parameter, $\sigma_a L_x$
τ_2: non-dimensional parameter, $\sigma_s L_x$
w: weighting constant

Subscripts
b: black body
B: bottom
e: exit of the porous matrix
g: gas
i: inlet of the porous matrix
p: solid
T: top

Superscripts
eq: equilibrium
in: incoming velocity direction
m: outgoing radiation direction
m': incoming radiation direction
out: outgoing velocity direction
$+$: downstream direction
$-$: upstream direction